We are IntechOpen,
the world's leading publisher of
Open Access books
Built by scientists, for scientists

6,900
Open access books available

185,000
International authors and editors

200M
Downloads

Our authors are among the

154
Countries delivered to

TOP 1%
most cited scientists

12.2%
Contributors from top 500 universities

Interested in publishing with us?
Contact book.department@intechopen.com

Numbers displayed above are based on latest data collected.
For more information visit www.intechopen.com

Electronic Properties of Deformed Graphene Nanoribbons

Guo-Ping Tong

Additional information is available at the end of the chapter

http://dx.doi.org/10.5772/51348

1. Introduction

As early as 1947, the tight-binding electronic energy spectrum of a graphene sheet had been investigated by Wallace (Wallace, 1947). The work of Wallace showed that the electronic properties of a graphene sheet were metallic. A better tight-binding description of graphene was given by Saito et al. (Saito et al., 1998). To understand the different levels of approximation, Reich et al. started from the most general form of the secular equation, the tight binding Hamiltonian, and the overlap matrix to calculate the band structure (Reich et al., 2002). In 2009, a work including the non-nearest-neighbor hopping integrals was given by Jin et al. (Jin et al., 2009).

It is common knowledge that a perfect grphene sheet is a zero-gap semiconductor (semimetal) that exhibits extraordinarily high electron mobility and shows considerable promise for applications in electronic and optical devices, high sensitivity gas detection, ultracapacitors and biodevices. How to open the gap of graphene has become a focus of the study. Early in 1996, Fujita et al. started to study the electronic structure of graphene ribbons (Fujita et al., 1996; Nakada et al., 1996) by the numerical method. The armchair shaped edge ribbons can be either semiconducting ($n=3m$ and $n=3m+1$, where m is an integer) or metallic ($n=3m+2$) depending on their widths, i. e., on their topological properties. First-principles calculations showed that the origin of the gaps for the armchair edge nanoribbons arises from both quantum confinement and the deformation caused by edge dangling bonds (Son et al., 2006; Rozhkov et al., 2009). This result implies that the energy gap can be changed by deformation. In 1997, Heyd et al. studied the effects of compressive and tensile, unaxial stress on the density of states and the band gap of carbon nanotubes (Heyd et al., 1997). Applying mechanical force (e.g., nanoindentation) on the graphene can lead to a strain of about 10%(Lee et al., 2008). Xiong et al. found that engineering the strain on the graphene planes forming a channel can drastically change the interfacial friction of water transport through it (Xiong et

al., 2011). Density functional perturbation theory is a well-tested *ab initio* method for accurate phonon calculations. Liu et al. (Liu et al., 2007) studied the phonon spectra of graphene as a function of uniaxial tension by using this theory. Edge stresses and edge energies of the armchair and zigzag edges in graphene also were studied by means of the theory (Jun, 2008). Jun found that both edges are under compression along the edge and the magnitude of compressive edge stress of armchair edge is larger than that of zigzag edge. By simulations of planar graphene undergoing in-plane deformations, Chung (Chung, 2006) found that crystal structures are different from the usual hexagonal configuration. The thermodynamic or kinetic character of the rearrangement was found to depend on the macroscopic straining direction. Neek-Amal et al. (Neek-Amal et al., 2010) simulated the bending of rectangular graphene nanoribbons subjected to axial stress both for free boundary and supported boundary conditions. Can et al. (Can et al., 2010) applied density-functional theory to calculate the equilibrium shape of graphene sheets as a function of temperature and hydrogen partial pressure. Their results showed that the edge stress for all edge orientations is compressive. Shenoy et al. (Shenoy et al., 2008) pointed out that edge stresses introduce intrinsic ripples in freestanding graphene sheets even in the absence of any thermal effects. Compressive edge stresses along zigzag and armchair edges of the sheet cause out-of-plane warping to attain several degenerate mode shapes and edge stresses can lead to twisting and scrolling of nanoribbons as seen in experiments. Marianetti et al. (Marianetti et al., 2010) reveals the mechanisms of mechanical failure of pure graphene under a generic state of tension at zero temperature. Their results indicated that finite wave vector soft modes can be the key factor in limiting the strength of monolayer materials. In the chemical activity of graphene, de Andres et al. (de Andres et al., 2008) studied how tensile stress affects σ and π bonds and pointed out that stress affects more strongly π bonds that can become chemically active and bind to adsorbed species more strongly. Kang et al. (Kang et al., 2010) performed a simulation study on strained armchair graphene nanoribbons. By comparison, those with strained wide archair nanoribbons can achieve better device performance. By combining continuum elasticity theory and tight-binding atomistic simulations, Cadelano et al. (Cadelano et al., 2009) worked out the constitutive nonlinear stress-strain relation for graphene stretching elasticity and calculated all the corresponding nonlinear elastic moduli. Gui et al. (Gui et al., 2008) found that graphene with a symmetrical strain distribution is always a zero band-gap semiconductor and its pseudogap decreases linearly with the strain strength in the elastic regime. For asymmetrical strain distributions the band gaps were opened at the Fermi level. This is because small number of k points is chosen (Farjam et al., 2009). We also investigated the energy spectrum and gap of wider graphene ribbons under a tensile force (Wei et al., 2009) and found that the tensile force can have the gap of the ribbon opened.

In this Chapter, we focus on the effects of deformed graphene sheets and nanoribbons under uniaxial stress on the electronic energy spectra and gaps based on the elasticity theory. Meanwhile, the energy spectrum of the curved graphene nanoribbons with the tubular warping is studied by the tight-binding approach. The energy spectrum of deformed graphene sheets subjected to uniaxial stress is given in Section 2. In Section 3, we discuss the electronic properties of graphene nanoribbons under uniaxial stress. The tubular warping deformation of graphene nanoribbons is presented in last Section.

2. Graphene under uniaxial stress

2.1. Elasticity theory

Since graphene is a monolayer structure of carbon atoms, when a force is exerted on it paral-
lel to its plane, the positions of the atoms will change with respect to some origin in space.
Let the x-axis be in the direction of the armchair edge of graphene and the y-axis in that of
the zigzag edge, as shown in Fig. 1. Let R and R' denote the positions of a carbon atom be-
fore and after deformation, respectively. According to the theory of elasticity, the relation
between the positions can be written in the form

$$\begin{pmatrix} R'_x \\ R'_y \end{pmatrix} = \begin{pmatrix} 1+\delta_1 & 0 \\ 0 & 1+\delta_2 \end{pmatrix} \begin{pmatrix} R_x \\ R_y \end{pmatrix} \tag{1}$$

where $\delta_1 = +\delta (\text{or} -\delta)$ is the tensile (or compression) stress along the x-direction and δ_2 is the
stress in the y-direction and small compared to δ_1, approximately equal to $\delta_1/6$. When the de-
formation of graphene occurs, the bond length between the carbon atoms changes and
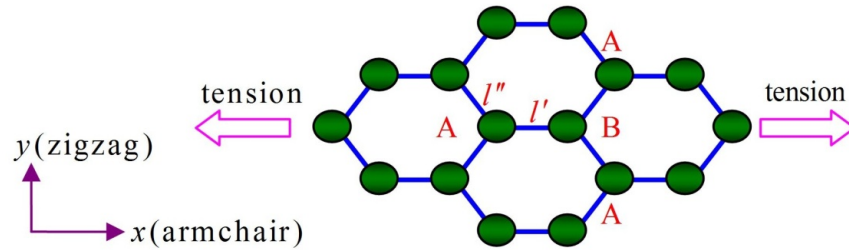which leads to the change of electronic hopping energies.

Figure 1. Graphene sheet subjected to the tensile stress in the x-direction. Symbols A and B denote sublattices with
two kinds of different carbon atoms, respectively. l' and l'' denote the bond lengths between tow adjacent carbon
atoms after deformation, respectively.

According to Harrison's formula (Harrison, 1980), the hopping energy after deformation is
expressed as follows

$$t' = \left(\frac{l_0}{l'} \right)^2 t_0 \tag{2}$$

where l_0 and t_0 denote the bond length and the hopping energy before deformation, respec-
tively. l' and t' are the bond length and the hopping energy after deformation, respectively.
From Fig. 1 and Eq. (1), the bond lengths between atoms A and B can be obtained

$$l' = R'_x = l_0(1+\delta),$$
$$l'' = \sqrt{R'^2_x + R'^2_y} = l_0\sqrt{1 + \frac{1}{4}\delta + \frac{13}{48}\delta^2} \tag{3}$$

The nearest neighbour hopping integrals associated with the bond lengths are

$$t' = \frac{t_0}{(1+\delta)^2}$$
$$t'' = \frac{t_0}{\left(1 + \frac{1}{4}\delta + \frac{13}{48}\delta^2\right)} \tag{4}$$

If graphene is subject to a tensile force in the y-direction, the hopping energies are given by

$$t' = \frac{t_0}{\left(1 - \frac{\delta}{6}\right)^2}$$
$$t'' = \frac{t_0}{\left(1 + \frac{17}{12}\delta + \frac{109}{144}\delta^2\right)} \tag{5}$$

2.2. The tight-binding energy spectrum

Let us now consider the band structure from the viewpoint of the tight-binding approximation. The structure of graphene is composed of two types of sublattices A and B as shown in Fig. 1. If $\varphi(r)$ is the normalized orbital $2p_z$ wave function for an isolated carbon atom, then the wave function of graphene has the form

$$|\psi\rangle = C_A|\psi_A\rangle + C_B|\psi_B\rangle \tag{6}$$

where

$$|\psi_A\rangle = \frac{1}{\sqrt{N}}\sum_A e^{ik\cdot R_A}|\varphi(r-R_A)\rangle$$

and

$$|\psi_B\rangle = \frac{1}{\sqrt{N}}\sum_B e^{ik\cdot R_B}|\varphi(r-R_B)\rangle \tag{7}$$

The first sum is taken over A and all the lattice points generated from it by primitive lattice translation; the second sum is similarly over the points generated from B. Here C_A and C_B are coefficients to be determined, R_A and R_B are the positions of atoms A and B, respectively, and N is the number of the unit cell in graphene. Substituting Eq. (6) in

$$H|\psi\rangle = E|\psi\rangle \tag{8}$$

we obtain the secular equation

$$\begin{vmatrix} H_{AA} - E & H_{AB} \\ H_{AB}^* & H_{AA} - E \end{vmatrix} = 0 \tag{9}$$

For the tensile stress in the x-direction, the solution to Eq.(9) is

$$E(k_x, k_y) = \pm\left[t'^2 + 4t't'' \cos\left(\frac{\sqrt{3}}{2}k_y R'_y\right)\cos\left(\frac{3}{2}k_x R'_x\right) + 4t''^2 \cos^2\left(\frac{\sqrt{3}}{2}k_y R'_y\right) \right]^{\frac{1}{2}} \tag{10}$$

where t' and t'' are the nearest-neighbour hopping integrals after deformation, given by Eq.(4).

Fig. 2 shows the electronic energy spectra of deformed graphene sheets for some high symmetric points Γ, M, and K under uniaxial stress. Because of uniaxial stress, the hexagonal lattice is distorted and the shape of the first Brillouin zone changes accordingly as the stress upon the lattice. Six "saddle" points on the boundary in the first Brillouin zone can be divided into two groups: M and M'. At the same time, Dirac point K will drift towards the saddle point M and is accompanied by a small angle. For the convenience of comparison, we give the spectrum of undeformed graphene in Fig. 2(a). From Fig. 2 (c) and (d), we see that tension along the armchair shape edge can reduce the band width at point Γ and increase the bandwidth at point M, and the result of compression is just opposite to that of tension. Fig. 2(e) tells us that tension along the zigzag shape edge can not only narrow the bandwidth at Γ point but decrease the bandwidth at M point as well. On the contrary, compression can simultaneously increase the bandwidth at Γ and M. Moreover, it may be seen from Fig. 2 that whether the tensile stress or compressive stress, the result of the high symmetric point M' is always opposite to that of the point M and the energy gap cannot be opened at Dirac point (K). On the other hand, we see yet that the energy band curves between M and M' for the graphene without stress are a straight line, but for the graphene with stress the curves are not. It appears to graphene that the uniaxial stress does not open the energy gap at Dirac point. When graphene is compressed along the armchair shape edge or extended along the zigzag shape edge a small energy gap is opened at K point, which is approximately equal to 0.1eV as the stress parameter takes to be 12%. From this reason, the graphene under uniaxial stress still is a semiconductor with the zero-energy gaps.
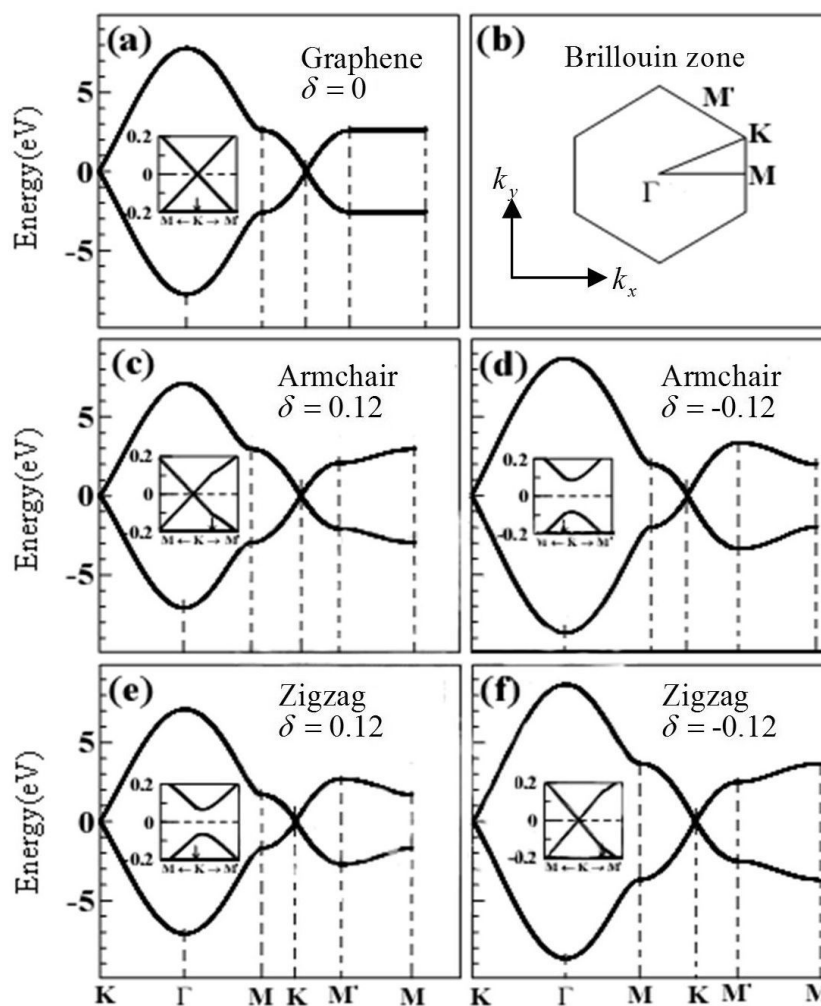
Figure 2. Electronic energy spectra of graphene under uniaxial tress for some high symmetric points.

3. Graphene nanoribbon under uniaxial stress

As mentioned in Section 2, for a graphene sheet subject to uniaxial stress there are no energy gaps at Dirac point. How to open the energy gaps of graphene? Studies showed that we can realize this goal by deducing the size of graphene, i.e., changing its toplogical propertiy(Son et al., 2006). On the other hand, the band gaps of graphene nanoribbons can be mamipulated by changing the bond lengths between carbon atoms, i.e., changing the hopping integrals, by exerting a strain force (Sun et al., 2008). The nearest-neighbor energy spectrum of an arm-chair nanoribbon was given by the tight-binding approach and using the hard-wall aboun-dary condition (Zheng et al., 2007). In the non-nearest-neighbor band structure of the nanoribbon was given by Jin et al (Jin et al., 2009). In this section we use the tight-binding approach to study the energy spectrum and gap of the nanoribbon under uniaxial stress along the length direction, i.e., x-direction, of the nanoribbon, as shown in Fig. 3.
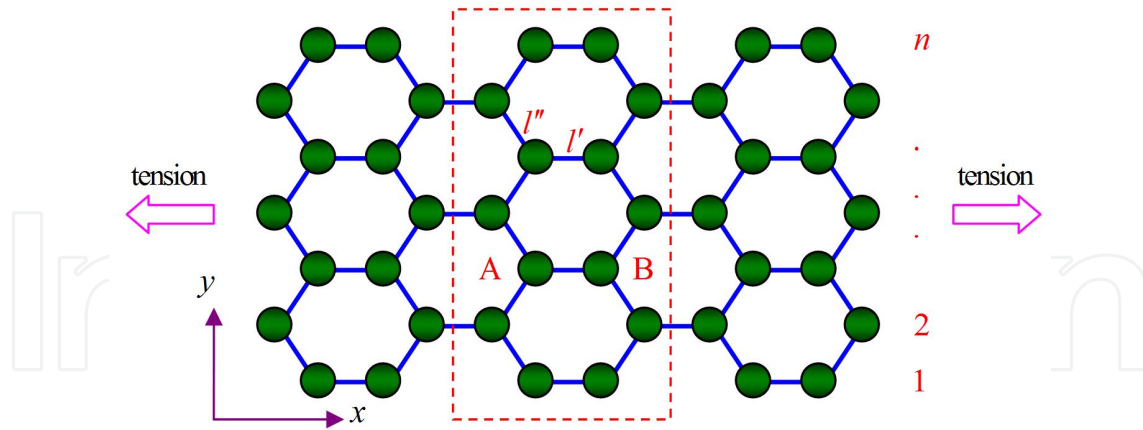
Figure 3. Structure of an armchair graphene nanoribbon with sublattices *A* and *B*. The tension is exerted on the nano-ribbon along the x-axis. Symbol *n* denotes the width of the nanoribbon. There are *n* sublatices *A* or *B* in a unit cell.

Since the unit cell of the nanoribbon has the translational symmetry in the *x*-direction, we can choose the plane-wave basis in the *x*-direction and take the stationary wave in the *y*-direction. For the armchair nanoribbon there are two kinds of sublattices *A* and *B* in a unit cell. Therefor, the wave functions of *A* and *B* sublattices in hard-wall conditions can be written as

$$|\psi_A(k_x, q)\rangle = \frac{1}{N_A} \sum_{j=1}^{n} \sum_{x_{A_j}} e^{ik_x x_{A_j}} \sin\left(\frac{\pi q}{(n+1)} j\right) |\varphi(r - R_{A_j})\rangle, \quad (q = 1, 2, \cdots, n)$$

$$|\psi_B(k_x, q)\rangle = \frac{1}{N_B} \sum_{j=1}^{n} \sum_{x_{B_j}} e^{ik_x x_{B_j}} \sin\left(\frac{\pi q}{(n+1)} j\right) |\varphi(r - R_{B_j})\rangle, \quad (q = 1, 2, \cdots, n)$$

(11)

where N_A and N_B are the normalized coefficients, $q = 1, 2, ..., n$ is the quantum number associated with the wave vector k_y, which denotes the discrete wave vector in the y-direction. When a graphene nanoribbon is subject to uniaxial stress, Eq.(11) still is available. For a nanoribbon, as long as the wave vector k_y in Eq.(10) is replaced by the discrete wave vector $k_y(q)$, we can obtain the energy dispersion relation of the form

$$E(k_x, q) = \pm \left[t'^2 + 4t''^2 \cos^2\left(\frac{q\pi}{n+1}\right) + 4t't'' \cos\left(\frac{q\pi}{n+1}\right) \cos\left(\frac{3}{2} k_x R'_x\right) \right]^{\frac{1}{2}}$$

(12)

Since the electronic energy spectrum of the perfect armchair nanoribbon depends strongly on the width of the nanoribbon, the different width has the different spectrum. For instance, the nanoribbon with widths *n*=3*m*+2 (*m* is an integer) is metallic and others are insulating. When we exert a tensile (or compressive) force on the nanoribbon along the x-axis, the metal nanoribbon is converted into an insulator or semiconductor.
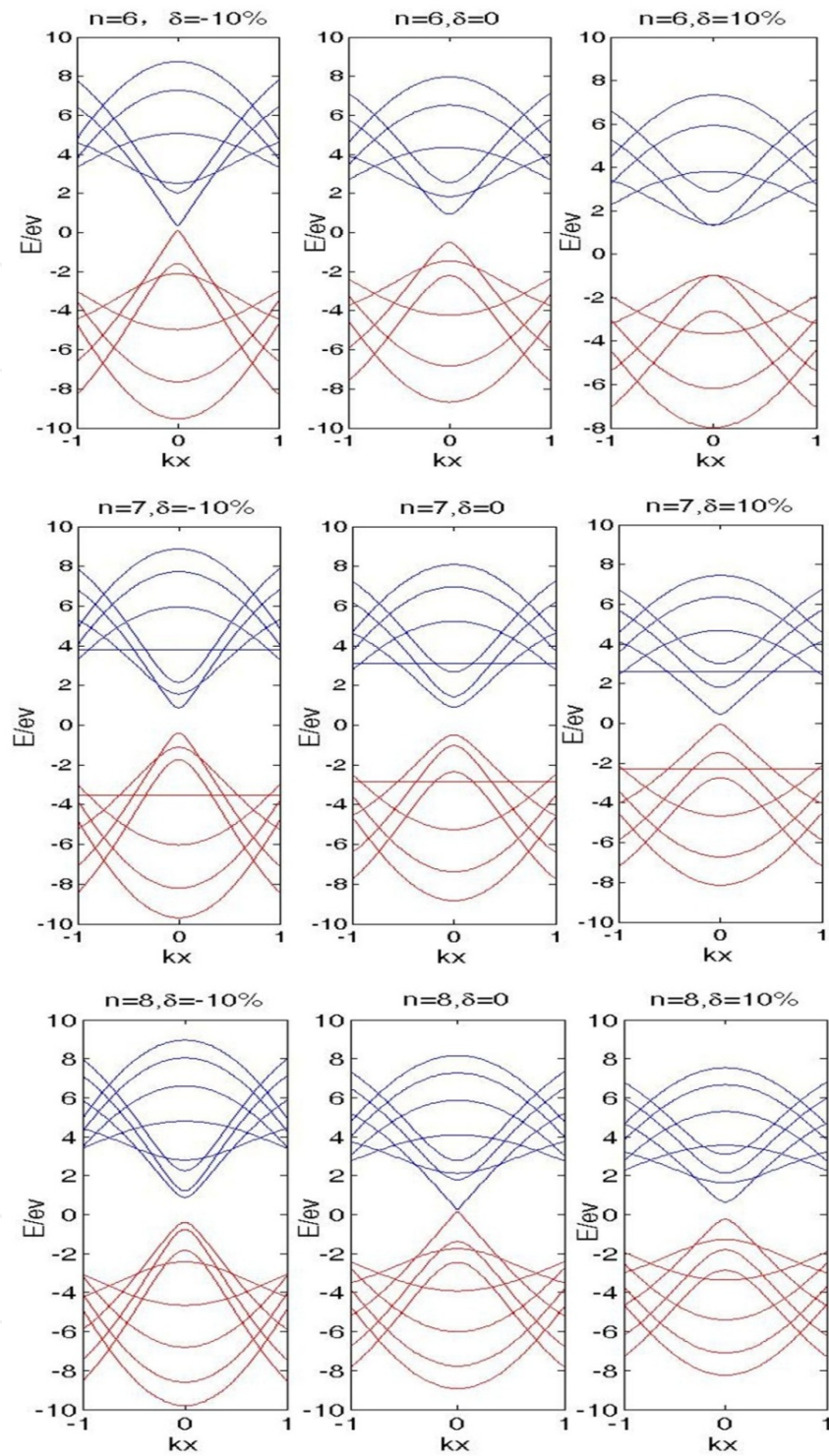
Figure 4. Band structures of armchair graphene nanoribbons under uniaxial stress with widths *n*=6, 7, 8. The stress parameterδis taken to be - 0.1, 0, and 0.1 respectively.

Fig. 4 shows the energy spectra of three kinds of the nanoribbons under uniaxial stress, and in which the next-nearest neighbor hopping integrals are taken into account. In order to facilitate comparison, the energy spectrum of the undeformed nanoribbon is given in Fig. 4. When

width $n=6$, the tensile stress can make the energy gap increase and the bandwidth decrease slightly. On the contrary, the compressive stress can decrease the gap and make the bandwidth widen. It is obvious that the energy band corresponding to quantum number $q=n-1=5$ plays an important role in the change of the band gap. When $n=7$, the tensile stress can make the gap narrow and the compressive stress has larger influence on the energy bandwidth, but not obvious on the gap. It can be seen that the energy band with quantum number $q=n-1=6$ contributes to the gap under compressive stress and which is clearly different from the tensile situation, where $q=n-2=5$. As for $n=8$, whether it is tensile or compression can open the gap and the energy band contributing to the gap belongs to quantum number $q=n-2=6$. It fallows from this that either tension or compression can change the gap and the bandwidth. Therefore, the electronic properties of armchair nanoribbons can be controlled by uniaxial stress.
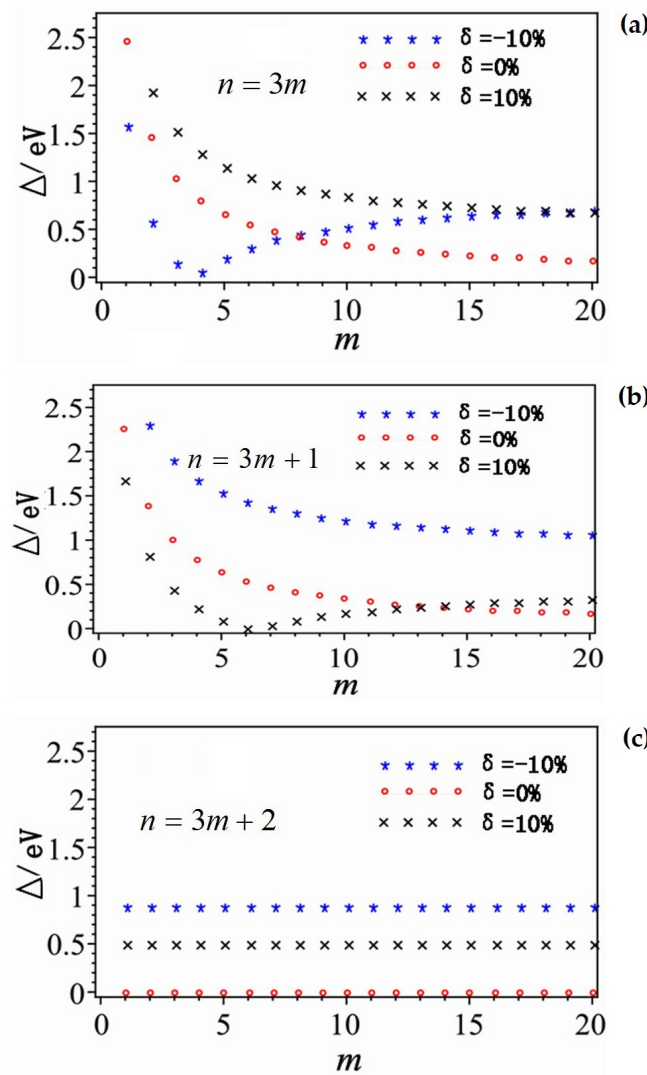

Figure 5. Energy gaps of deformed armchair nanoribbons as a function of the width n (m). SymbolΔdenotes the energy gap. The stress parameter$\delta$is taken to be -0.1, 0, and 0.1.

When the stress is constant, three graphs of the energy gaps with the width of the nanorib-bon changes are shown in Fig. 5, where (a) the width n is equal to $3m$, (b) $n=3m+1$, and (c) $n=3m+2$. The results shown in Fig. 5 are inclusive of the nearest-neighbor hopping integrals. We see from Fig. 5(a) that the compressive stress can make an inflection point of the band gap minimum for the $3m$-type nanoribbon and the width corresponding with the inflection point is about 12, and the tensile stress can not make a minimum value of the gap. For the $3m+1$-type nanoribbon, the result shown in Fig. 5(b) tells us that the tensile stress also can produce the minimum value of the gap and the corresponding width is 19. In the case of the $3m+2$-type nanoribbon, tensile or compression does not change the energy gap (see Fig. 5(c)). Furthermore, we found by calculations that with the inclusion of the next-nearest neighbor and the third neighbor respectively, the minimum point of the gap moves toward the direction of the origin of coordinates (zero width), i.e., the width of the non-nearest-neighbor hopping is less than that of the nearest neighbor.

On the other hand, in order to make certain of the relationship between the gap and the stress, the curves of the gap versus the stress are given in Fig. 6. As shown in Fig. 6, the gap increases as the stress increases for the $3m$- and $3m+1$-type nanoribbons and changes in the V-shaped curve for the $3m+2$-type nanoribbon.
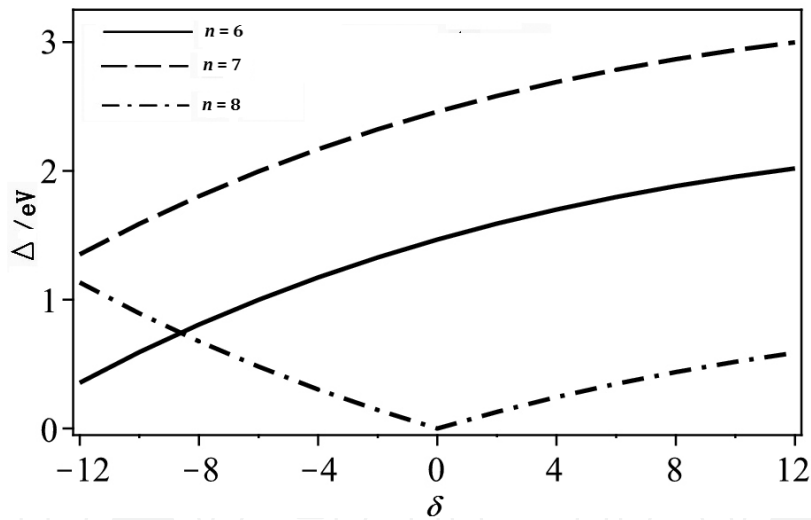

Figure 6. Energy gaps of deformed armchair nanoribbons as a function of stressδ. SymbolΔdenotes the energy gap. Solid, dashed, and dotted lines denote widths $n=6$, $n=7$, and $n=8$, respectively.

Figure 7. A curved armchair graphene nanoribbon with the tubular shape. $\theta$is the central angle and $r$is the curved radius of the nanoribbon.

4. The tubular warping graphene nanoribbon

4.1. Theoretical Model

In this section we choose an armchair ribbon as an example and which is bent into the tubular shape (cylindrical shape), as shown in Fig. 7. This tubular ribbon still has the periodicity in its length direction, but its dimensionality has changed. The consequence of such a dimension change is to lead to the change of the electronic energy dispersion relation. This is because the sp^2 hybridization of a flat ribbon turns into the sp^3 hybridization of a curved ribbon, i.e., the curvature of graphene nanoribbons will result in a significant rehybridization of the π orbitals (Kleiner et al., 2001). From this reason, the s-orbital component must be taken into account in calculating electronic energy bands.

Because of the curl of the ribbon, the wavefunction of π electrons should be composed of the s- and p-orbital components. The wavefunctions of sublattices A and B in cylindrical coordinates are written then

$$|\psi_A\rangle = \frac{1}{N_A}\sum_{j=1}^{n}\sum_{z_{A_j}} e^{ik_z z_{A_j}} \sin\left(j\frac{\sqrt{3}}{2}k_\phi a\right)\left[\sqrt{c_j}\left|s_{A_j}\right\rangle + \sqrt{1-c_j}\left|p_{z A_j}\right\rangle\right]$$ (13)

$$|\psi_B\rangle = \frac{1}{N_B}\sum_{j=1}^{n}\sum_{z_{B_j}} e^{ik_z z_{B_j}} \sin\left(j\frac{\sqrt{3}}{2}k_\phi a\right)\left[\sqrt{c_j}\left|s_{B_j}\right\rangle + \sqrt{1-c_j}\left|p_{z B_j}\right\rangle\right]$$ (14)

where c is the s-orbital component of electrons, given by (Huang et al., 2006; 2007)

$$c = \frac{2\sin^2\beta}{1-\sin^2\beta}$$ (15)

and

$$\beta = \frac{a}{4\sqrt{3}r}$$ (16)

Here β is a small inclined angle (Kleiner et al., 2001) between the p_z orbital and the normal direction of the cylindrical surface, r is the radius of the cylindrical surface, and a is the distance between two adjacent carbon atoms.

4.2. Results and Discussion

To clearly understand the effect of curvature, we choose the width n=6, 7, and 8 respectively as examples to show the characteristics of their electronic energy spectra. On the other hand,

in order to compare with the ideal flat nanoribbon, the results of the ideal ribbon along with the tubular warping ribbon are also given in Fig. 8, where black lines denote the ideal ribbon and red lines are the tubular warping ribbon.
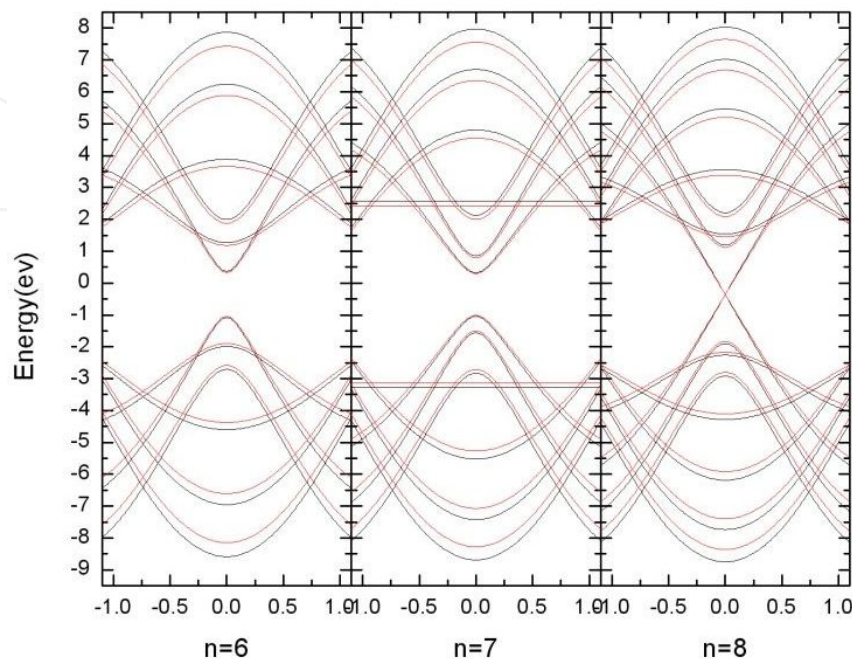

Figure 8. Band structures of the curved armchair nanoribbons with widths n = 6, n = 7, and n = 8, respectively. Black lines are the energy band of a perfect nanoribbon and red lines denote the band of a curved nanoribbon with the tubular shape.

By comparison, we found that the energy bandwidths become narrowed obviously for the widths n=6, 7, 8 and then this bending does not nearly influence on the energy gaps. This is because the localization of electrons is enhanced from two-dimensional plane to three-dimensional curved surface. When n=6, the increment of the gap with respect to the flat ribbon is equal to 0.074eV. When n=7, the change of the gap is 0.065eV. As for n=8, its metallic behavior does not change as the ribbon is rolled up. Fig. 9 illustrates the density of states of the warping ribbons with widths n=6, 7, 8. The meaning of the black and red lines in Fig. 9 is the same as in Fig. 8. From Fig. 9, we see that the tubular warping is responsible for the energy bandwidth narrowing. The density of states of both the top of the valence band and the bottom of the conduction band does not nearly change. It follows that this warping ribbon still keeps all the characteristics of the flat ribbon, especially for n=7. This means that the change of this dimension does not affect the electronic structure seriously. This is why we usually use a graphene sheet to study the electronic structure of a carbon nanotube. In addition, in order to show the effect of the curvature on the energy gap, a graph of the gap varying with the central angle is plotted in Fig. 10. It is apparent that for a fixed width the gap has a maximum value as the increasing of the central angle. When n=6, the central angle corresponding to the maximum value is between $5\pi/4$ and $3\pi/2$. When n=7, this angle approximately equals $3\pi/2$. As the central angle is equal to zero, the warping ribbon becomes a flat ribbon and as the central angle goes to 2π, the warp-

ing ribbon becomes a carbon nanotube. Fig. 10 also shows such a fact that when a graphene nanoribbon is bent into a nanotube, its energy gap is increased.
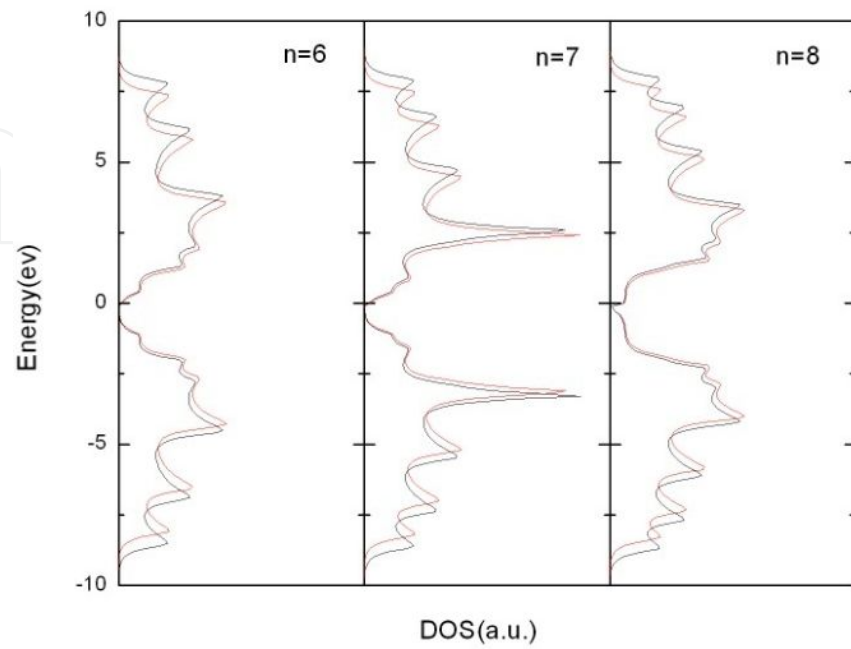

Figure 9. Density of states of tubular warping armchair nanoribbons. Black and red lines are the flat and warping nanoribbons, respectively.
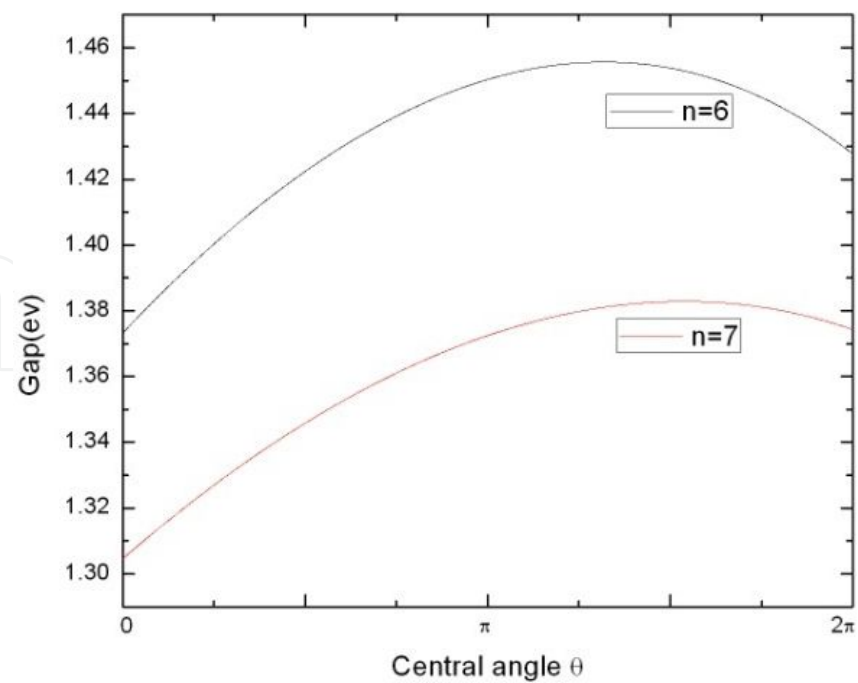

Figure 10. Energy gaps as a function of the central angle (or curvature).

5. Graphene nanoribbon modulated by sine regime

A free standing graphene nanoribbon could have out-of-plane warping because of the edge stress (Shenoy et al., 2008). This warping will bring about a very small change of the electronic energy spectrum. An ideal graphene nanoribbon only has periodicity in the direction of its length and there is no periodicity in the y-direction. To show the periodic effect in the y-direction, we modulate it with the aid of a sine periodic function

$$z = A\sin(fy) \tag{17}$$

where A is the modulation amplitude and f denotes the modulation frequency, i.e., modulated number per unit length. The modulated graph of an armchair graphene nanoribbon is shown in Fig. 11.
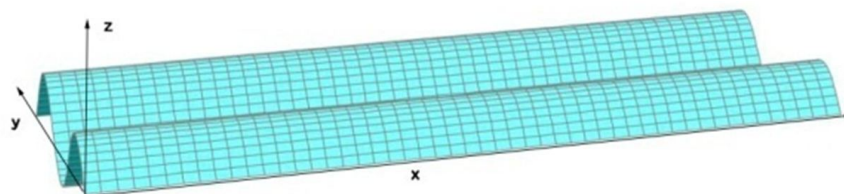

Figure 11. Graphene nanoribbon modulated by sine regime in the direction of the width.
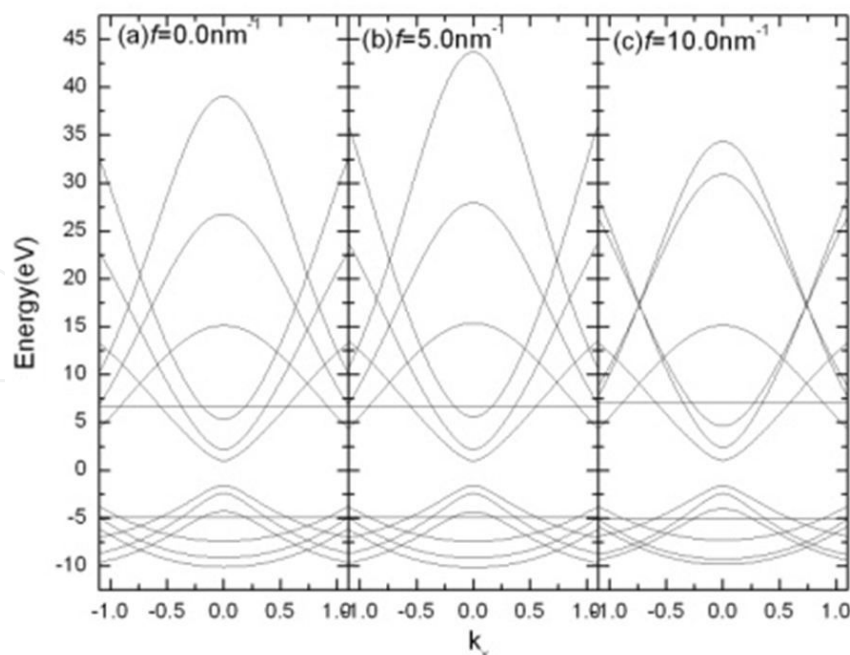

Figure 12. Energy spectra of graphene nanoribbons with width n=7 modulated by sine regime in the direction of the width. f is the modulation frequency.

By numerical calculations, we found that different modulation frequencies have different electronic band structures, i.e., the energy band structures depend strongly on the modulation frequency f and the modulation amplitude A. We take the width n=7 as an example to calculate the electronic energy spectrum. When the amplitude A is fixed, the energy band structures with different frequencies are shown in Fig. 12. It may be seen from Fig. 12 that this periodic modulation does not damage the Dirac cones, i.e., the topological property of armchair graphene nanoribbons is not destroyed. On the other hand, Fig. 12 tells us that this periodic modulation can change the energy band structure, i.e., both the bandwidth and band gap can be controlled by the modulation frequency. The density of states of electrons for an armchair graphene nanoribbon with n=7, modulated by using a sine function along the width direction, is plotted in Fig. 13.
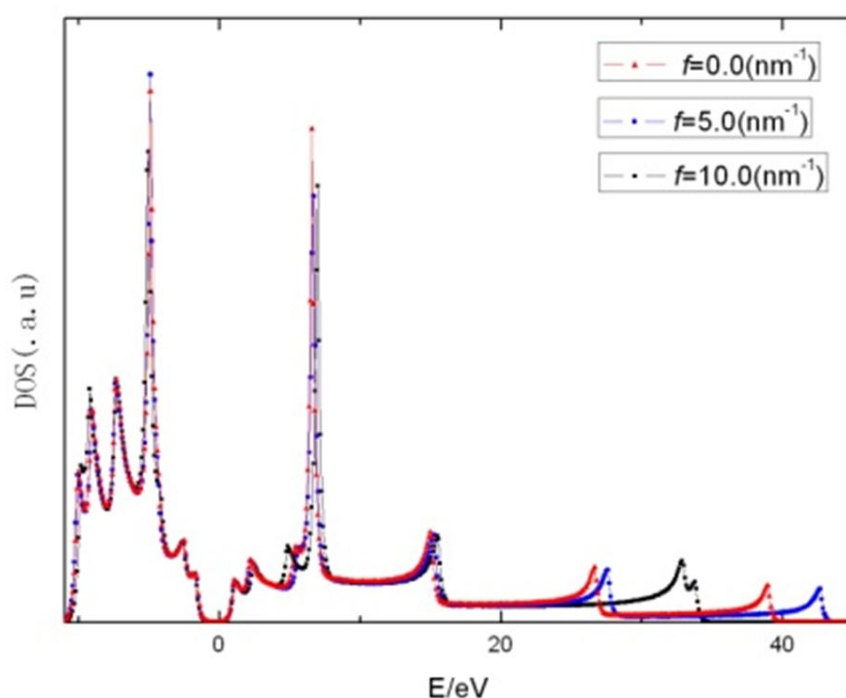

Figure 13. Density of states of graphene nanoribbons with width n=7 modulated by sine regime in the direction of the width.

When the modulation amplitude, taken to be 0.1nm, is fixed, different modulation frequencies have slightly different densities of states of electrons. The main difference between the frequencies 0.0nm^{-1}, 5.0nm^{-1}, and 10.0nm^{-1} is in the conduction band and the density of states of the valence band is the same nearly. It follows that the modulation along the width direction of the ribbon makes a notable impact for the density of states of the conduction band, especially for the high energy band corresponding to the standing wave of the smaller quantum number. In order to reveal the effect of the modulation amplitude on the electronic properties, the energy bands for the different amplitudes are calculated under certain frequency. Fig. 14 shows the band structures of the different amplitudes A=0.0nm, A=0.05nm, and A=0.1nm for an armchair nanoribbon with n=7, where the frequency f is taken to be

10nm^{-1}. When the modulation amplitude A=0.1nm, the band gaps corresponding to frequencies f=0.0nm^{-1}, 5nm^{-1}, and 10nm^{-1} are 2.580eV, 2.600eV, and 2.666eV, respectively. It seems that the band gaps linearly increase as the frequency increases. In fact, the inflection point of the smallest gap appears at f=6.02nm^{-1}, where the gap is equal to 2.571eV. There are other inflection points of the gap as the frequency increases, but the gaps of these points are big compared to that of the lowest inflection point (see Fig. 15(b)).
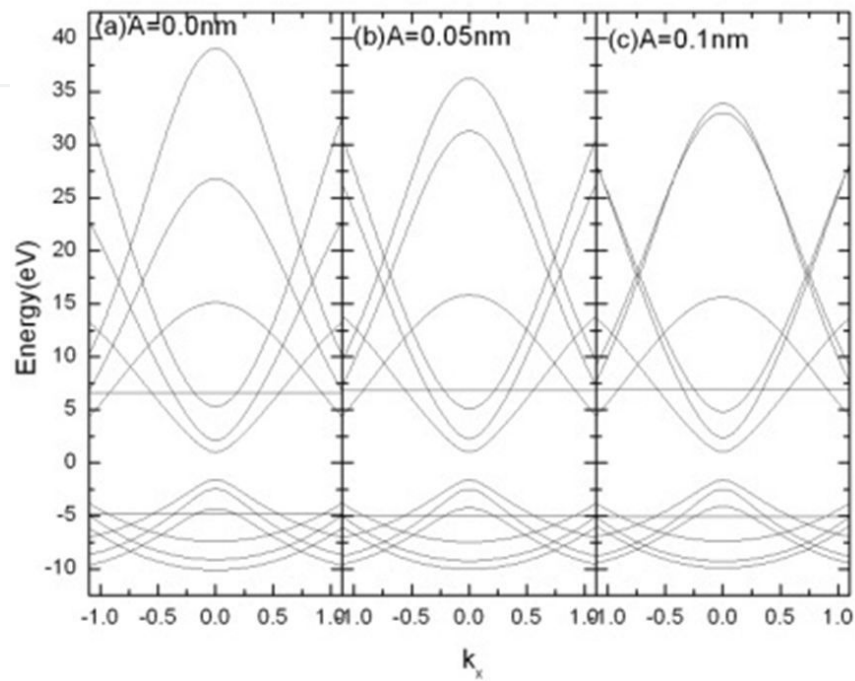

Figure 14. Energy spectra of graphene nanoribbons with width n=7 modulated by sine regime in the direction of the width. The modulation frequency f is taken to be 10nm^{-1} and A is the modulation amplitude.
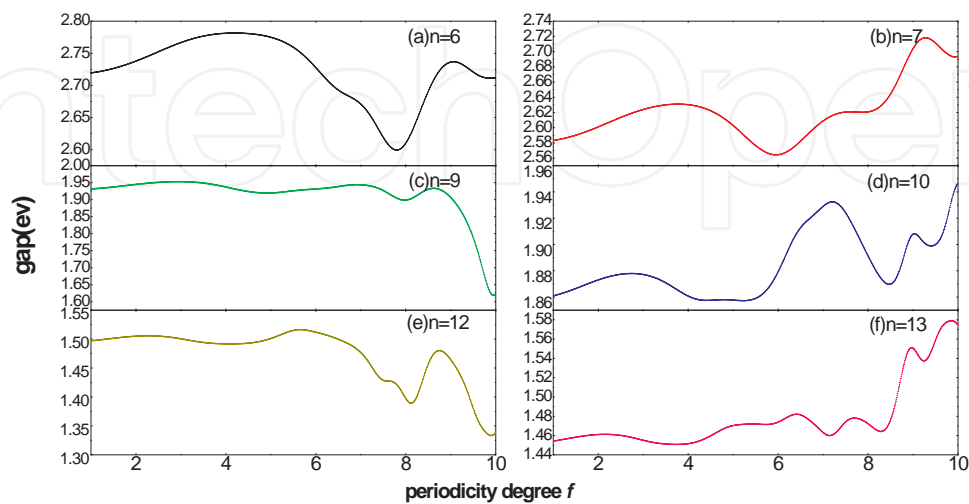

Figure 15. Energy gaps as a function of the modulation frequency f.

6. Conclusion

We investigated the electronic energy spectra of graphene and its nanoribbon subject to un-axial stress within the tight-binding approach. The unaxial stress can not open the energy gap of graphene at Dirac point K. But compression along the armchair shape edge or exten-sion along the zigzag shape edge will make a small energy gap opened at K point. From this reason, the graphene subject to uniaxial stress still is a semiconductor with the zero-energy gaps. The position of Dirac point will vary as the stress. For the armchair graphene nanorib-bon, the tensile or compressive stress not only can transfer the metallicity into the semicon-ductor, but also have the energy gap increased or decreased and the energy bandwidth widened or narrowed. Therefore, we can use the unaxial stress to control the electronic properties of armchair graphene nanoribbons. In addition, the tubular warping deformation of armchair nanoribbons does not nearly influence on the energy gap, but it is obvious to effect on the bandwidth. In addition, we also studied the periodic modulation of the shape of armchair nanoribbons by sine regime. This modulation can change its electronic proper-ties. For the other modulation manner, we no longer discuss it here.

The advantage of the tight-binding method is that the physical picture is clearer and the cal-culating process is simpler compared to the first-principles calculations. This method is suit-able only for narrow energy bands. Because graphene nanoribbons are the system of wider energy bands, this method has its limitation.

Author details

Guo-Ping Tong[*]

Address all correspondence to: tgp6463@zjnu.cn

Zhejiang Normal University, China

References

[1] Cadelano, E., Palla, P. L., Giordano, S., & Colombo, L. (2009). Nonlinear elasticity of monolayer graphene. *Phys. Rev. Lett.*, 102(23), 235502-4.

[2] Can, C. K., & Srolovitz, D. J. (2010). First-principles study of graphene edge proper-ties and flake shapes. *Phys. Rev. B*, 81(12), 125445-8.

[3] Chung, P. W. (2006). Theoretical prediction of stress-induced phase transformations of the second kind in graphene. *Phys. Rev. B*, 73(7), 075433-5.

[4] de Andres, P. L., & Vergés, J. A. (2008). First-principles calculation of the effect of stress on the chemical activity of graphene. *Applied Physics Letters*, 93(17), 171915-3.

[5]   Farjam, M., & Rafii-Tabar, H. (2009). Comment on "Band structure engineering of graphene by strain: First-principles calculations". *Phys. Rev. B*, 80(16), 167401-3.

[6]   Feyd, R., Charlier, A., & Mc Rae, E. (1997). Uniaxial-stress effects on the electronic properties of carbon nanotubes. *Phys. Rev. B*, 55(11), 6280-6824.

[7]   Fujita, M., Wakabayashi, K., Nakada, K., & Kusakabe, K. (1996). Peculiar localized state at zigzag graphite edge. *J. Phys. Soc. Jpn.*, 65(7), 1920-1923.

[8]   Gui, G., Li, J., & Zhong, J. X. (2008). Band structure engineering of graphene by strain: First-principles calculations. *Phys. Rev. B*, 78(7), 075435-6.

[9]   Harrison, W. A. (1980). *Electronic structure and properties of solids*, San Francisco, Freeman.

[10] Huang, Q. P., Yin, H., & Tong, G. P. (2006). Effect of π orbital orientations on the curvature and diameter of single-wall carbon nanotubes. *Journal of Atomic and Molecular Physics*, 23(4), 704-708.

[11] Huang, Q. P., Tong, G. P., & Yin, H. (2007). Calculation of the hybridization orbital of single-wall carbon nanotubes. *Journal of Atomic and Molecular Physics*, 24(1), 45-50.

[12] Jin, Z. F., Tong, G. P., & Jiang, Y. J. (2009). Effect of the non-nearest-neighbor hopping on the electronic structure of armchair graphene nanoribbons. *Acta Physica Sinica*, 58(12), 8537-8543, 1000-3290.

[13] Jun, S. (2008). Density-functional study of edge stress in graphene. *Phys. Rev. B*, 78(7), 073405-4.

[14] Kang, J. H., He, Y., Zhang, J. Y., Yu, X. X., Guan, X. M., & Yu, Z. P. (2010). Modeling and simulation of uniaxial strain effects in armchair graphene nanoribbon tunneling field effect transistors. *Applied Physics Letters*, 96(25), 252105-3.

[15] Kleiner, A., & Eggert, S. (2001). Curvature, hybridization, and STM images of carbon namotubes. *Phys. Rev. B*, 64(11), 113402-4.

[16] Lee, C., Wei, X., Kysar, J. W., & Hone, J. (2008). Measurement of the elastic properties and intrinsic strength of monolayer graphene. *Science*, 321(5887), 385-388.

[17] Liu, F., Ming, P. B., & Li, J. (2007). Ab initio calculation of ideal strength and phonon instability of graphene under tension. *Phys. Rev. B*, 76(6), 064120-7.

[18] Marianetti, C. A., & Yevick, H. G. (2010). Failure mechanisms of graphene under tension. *Phys. Rev. Lett.*, 105(24), 245502-4.

[19] Nakada, K., Fujita, M., Dresselhaus, G., & Dresselhaus, M. S. (1996). Edge state in graphene ribbons: Nanometer size effect and edge shape dependence. *Phys. Rev. B*, 54(24), 17954-17961, 1550-235X.

[20] Neek-Amal, M., & Peeter, F. M. (2010). Graphene nanoribbons subjected to axial stress. *Phys. Rev. B*, 82(8), 085432-6.

[21] Reich, S., Maultzsch, J., & Thomsen, C. (2002). Tight-binding description of graphene. *Phys. Rev. B*, 66(3), 035412-5.

[22] Rozhkov, A. V., Savel'ev, S., & Nori, F. (2009). Electronic properties of armchair graphene nanoribbons. *Phys. Rev. B*, 79(12), 125420-10.

[23] Saito, R., Dresselhaus, D., & Dresselhaus, M. S. (1998). *Physical Properties of Carbon Nanotubes*, Imperial College Press, 1-86094-093-5, London.

[24] Shenoy, V. B., Reddy, C. D., Ramasubramaniam, A., & Zhang, Y. W. (2008). Edge-stress- induced warping of graphene sheets and nanoribbons. *Phys. Rev.Lett.*, 101(24), 245501-4.

[25] Son, Y. W., Cohen, M. L., & Louie, S. G. (2006). Energy gaps in graphene nanoribbons. *Phys. Rev. Lett.*, 97(21), 216803-4.

[26] Sun, L., Li, Q., Ren, H., Su, H., Shi, Q., & Yang, J. (2008). Strain effect on electronic structures of graphene nanoribbons : A first-principles study. *The Journal of Chemical Physics*, 129(7), 074704.

[27] Wallace, P. R. (1947). The band theory of graphite. *Phys. Rev.*, 71(9), 622-634.

[28] Wei, Y., & Tong, G. P. (2009). Effect of the tensile force on the electronic energy gap of graphene sheets. *Acta Physica Sinica*, 58(3), 1931-1934.

[29] Xiong, W., Zhe, Liu. J., , M., Xu, Z. P., Sheridan, J., & Zheng, Q. S. (2011). Strain engineering water transport in graphene nanochannels. *Phys. Rev. E*, 84(5), 056329-7.

[30] Zheng, H. X., Wang, Z. F., Luo, T., Shi, Q. W., & Chen, J. (2007). Analytical study of electronic structure in armchair graphene nanoribbons. *Phys. Rev. B*, 75(16), 165411-6.